On the efficiency of energy harvesters

A classification of dynamics in miniaturized generators under low-frequency excitation

Blad, Thijs; Tolou, Nima

DOI
10.1177/1045389X19862621

Publication date
2019

Document Version
Final published version

Published in
Journal of Intelligent Material Systems and Structures

Journal of Intelligent Material Systems and Structures

Original Article

Journal of Intelligent Material Systems and Structures
2019, Vol. 30(16) 2436–2446

DOI: 10.1177/1045389X19862621
journals.sagepub.com/home/jim


On the efficiency of energy harvesters: A classification of dynamics in miniaturized generators under low-frequency excitation

Thijs WA Blad and Nima Tolou

Abstract

Although motion energy harvesting at the small scales has been a research topic for over 20 years, the implementation of such generators remains limited in practice. One of the most important contributing factors here is the poor performance of these devices under low-frequency excitation. In this research, a new metric is proposed to evaluate the performance and bandwidth of generators at low frequencies. For that, a classification based on the dynamics was made. It was found that the highest efficiencies were found in single-degree-of-freedom resonators where a large motion amplification was achieved. Smaller generators can be designed by limiting the motion through end-stops at the cost of a reduced efficiency. Moreover, it was argued that upon miniaturization, resonators could be outperformed by generators using a frequency up-conversion principle.

Keywords

Energy harvesting, non-linear dynamics, frequency up-conversion, low-frequency

1. Introduction

Motion energy harvesting with miniaturized devices has been studied for over 20 years since the early work of Williams and Yates (1996), in which the piezoelectric, electromagnetic, and electrostatic transduction mechanisms were investigated for the purpose of vibration-to-electric energy conversion. Devices that incorporate such transduction mechanisms are called motion energy harvesters and have received much interest as they may provide an alternative to batteries. Especially, for biomedical applications such as pacemakers, hearing aids, insulin pumps and various sensors, the elimination of a dependency on batteries can offer a huge quality of life improvement to patients. Despite the vast amount of research on the topic, the implementation of miniaturized motion energy harvesters remains limited in practice (Daqaq et al., 2014). One of the main contributing factors is that the performance of these systems is poor when excited by a low-frequency driving motion such as human motion (<10 Hz) (Green et al., 2013).

In prior art, a few design strategies were proposed to effectively harvest energy from these low-frequency motions. Bowers and Arnold (2009) argued that the commonly used resonant generators need to be very large to be effective at low frequencies. As an alternative, a 4 cm^3 concept based on rolling magnets was proposed for which an average output power of 1.44 mW was shown when carried in a pocket during running. Galchev et al. (2012) developed a piezoelectric system based on the frequency up-conversion principle pioneered by Kulah and Nafaji (2008). The 3.75 cm^3 prototype was able to generate an average power of 13.6 μW from a vibration of 10 Hz at 1 g. In the work of Geisler et al. (2017), non-linearities are introduced to constrain the internal motion and limit the size of generator. Excited by a 6 Hz vibration at 2 g, the 9 cm^3 prototype showed an average power of 6.57 mW. It was estimated that only up to 36% of the theoretical power output was attainable as a result of the displacement constraints.

However, with the existing methods it is not possible to generalize the results from these studies and compare the performances of the used design strategies on an

Department of Precision and Microsystems Engineering, Delft University of Technology, The Netherlands

Corresponding author:
Thijs WA Blad, Department of Precision and Microsystems Engineering, Delft University of Technology, 2628 CD Delft, The Netherlands.
Email: t.w.a.blad@tudelft.nl

abstract level. Without such a proper comparison, it remains unclear what specific challenges need to be solved to achieve a high efficiency. The research objective of this work is to classify these generators by their dynamics and compare the efficiencies between the groups. For this purpose, a new metric will be proposed. First, the metric presents a modification to an existing efficiency metric that adds a sensitivity to generator shape and material. Second, a new parameter is introduced which is called the motion ratio and relates the excitation amplitude to the dimension of the generator in the direction of the driving motion.

In section "Methods," the methods are explained and the new metrics are introduced. Section "Classification of generator dynamics" presents the classification, and section "Results" presents the results of the reported generators and identifies the respective groups. Section "Discussion" discusses the observations that can be made from the results, and the conclusions are presented in section "Conclusion."

2. Methods

2.1. Performance evaluation

For the comparison of different devices or harvesting strategies, there are a number of performance metrics available. Excellent investigations and discussions of these metrics were presented by Mitcheson et al. (2008) and Liu et al. (2015a). The *volume figure of merit* (FoM_V) was introduced as a metric that could make a fair comparison between different types and sizes of generators under different vibration conditions. This metric compares the useful power output of a generator with the power output of an imaginary generator cube of the same volume, V, driven by the same vibration conditions. To set a baseline, the proof mass of this generator is assumed to be made from gold.

Although the FoM_V normalizes the output power to the total volume, the shape of this volume is not taken into account. This is a problem because the power output of the generator scales with $P \propto L^2$ in the direction of the driving motion and $P \propto L$ in the perpendicular dimensions (Mitcheson et al., 2008). Consider the example of Figure 1, where two imaginary generators are sketched with an equal volume, V, and mass, M. In this example, a larger power output can be expected from the cylindrical generator due to its greater L_z dimension. This leads to an unfair comparison where some designs are already ahead in terms of FoM_V due to their shape, regardless of their dynamic performance.

In order to make this comparison more fair, a variation in the FoM_V is proposed, which will be named the generator figure of merit (FoM_G). In this metric, the $V^{4/3}$ is replaced by the product VL_z, to take into account both the volume and the shape of the generator. Furthermore, the real density of the proof mass material is included instead of the density of gold. This ensures that the efficiency fully depends on the design of the generator and not on the selection and/or availability of the proof mass material. The following expression is obtained

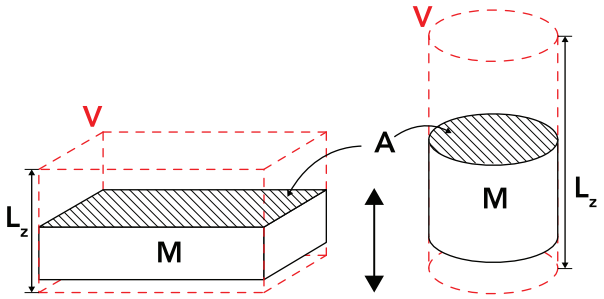

Figure 1. Two imaginary generators with an equal total volume, V, and mass, M. A greater power output can be expected from the cylindrical generator due to its larger dimension in the direction of the driving motion, L_z.

$$\mathrm{FoM}_G = \frac{P_{\mathrm{avg}}}{\frac{1}{16} Y_0 \rho_M V L_z \omega^3} \times 100\% \tag{1}$$

where Y_0 and ω are the amplitude and frequency of the driving motion, V is the total volume occupied by the device, L_z is the dimension of the generator along the direction of the applied motion, ρ_M is the density of the proof mass material, and P_{avg} is the average output power.

2.2. Peak efficiency and normalized half-efficiency bandwidth

In a great deal of the experimental work, the power output of a generator prototype is presented for a range of input conditions, typically through frequency sweep (with constant acceleration). From these data, a frequency-efficiency graph can be constructed by calculating equation (1) for every data point, as shown in Figure 2. For the assessment of the performance of the generators, two properties will be evaluated: the peak efficiency, η_{pk}, and the normalized half-efficiency bandwidth, BW_{nhe}. In contrast to previous metrics, the peak performance and bandwidth are therefore derived from the efficiency as calculated by the FoM_G instead of from the raw output power.

The peak efficiency (η_{pk}) is defined as the maximum efficiency obtained by the generator. Please note that this point does not necessarily coincide with the point at which a maximum output power is achieved. Although a fair comparison can be made between the efficiencies of different designs, η_{pk} only reflects the maximum efficiency at one particular frequency. Therefore, no bandwidth information is included in this property.

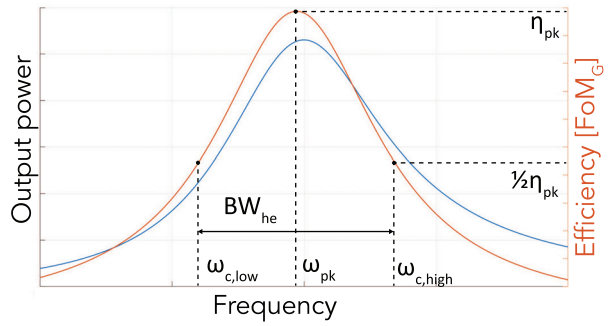

Figure 2. Example frequency-output power (blue) and frequency-efficiency graph (orange) of an energy harvester. The peak efficiency, η_{pk}, and normalized half-efficiency bandwidth, BW_{nhe}, indicated in the figure are important properties for the performance evaluation of the generator.

For this reason, a second property is derived from the frequency–efficiency graph. The normalized half-efficiency bandwidth (BW_{nhe}) is defined by the following expression

$$BW_{nhe} = \frac{BW_{he}}{\omega_{pk}} = \frac{\omega_{c,high} - \omega_{c,low}}{\omega_{pk}} \quad (2)$$

where BW_{he} is the half-efficiency bandwidth between the higher ($\omega_{c,high}$) and lower ($\omega_{c,low}$) corner frequencies and ω_{pk} is the frequency at which η_{pk} is found.

2.3. The motion ratio

The dynamics of the energy harvester are for a great deal determined by the L_z dimension of the generator and the amplitude of the driving motion, Y_0. For example, many generators make use of resonance induce an relative displacement that is greatly amplified w.r.t. the amplitude of the driving motion (Roundy, 2005). Naturally, these dynamics are only possible if $L_z >> Y_0$ for obvious reasons. Therefore, it is proposed here to look at the ratio between the vibration amplitude and this dimension. This ratio is defined here as the motion ratio, λ, of the generator

$$\lambda = \frac{L_z}{2Y_0} \quad (3)$$

2.4. Literature search method

Relevant scientific literature on the topic of energy harvesting was searched in the database of Scopus. Only publications of experimental nature where both λ and the FoM_G could be found are included in the dataset. This means that the relevant parameters were directly reported, could be calculated, or could be estimated from graphs or figures. For example, the generator volume was stated directly or calculated based on the reported dimensions of the device. Sometimes, a particular design was tested under multiple conditions and therefore appears multiple times in the table, with different λ and FoM_G. It should be noted that the dataset is predominantly oriented toward generators operating at a frequency below 100 Hz, because it was expected that low motion ratios would rarely be found at higher frequencies due to small vibration amplitudes ($Y_0 \propto 1/\omega^2$). Moreover, it should be noted that a great portion of the literature fails to report a complete set of the important parameters of the generator and the testing conditions required to calculate the FoM_G. The dataset reported here is therefore only a fraction of the total amount of experimental work.

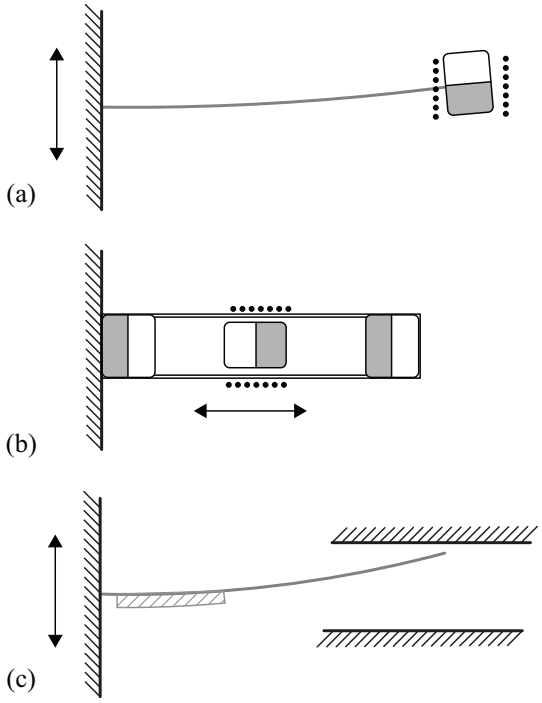

Figure 3. Sketches of single-degree-of-freedom energy harvesters: (a) without end-stops, (b) with magnets acting as soft-stops, and (c) with mechanical contacts acting as hard-stops.

3. Classification of generator dynamics

Based on the dynamics found in the reported energy harvesters, a classification is proposed where the generators are split in the following groups. The designs found in the literature are sketched and grouped in Figures 3 and 4 according to the classification.[1]

3.1. Single-degree-of-freedom generators

This subsection groups all energy harvesters that have a single degree-of-freedom (SDoF), which is used directly for energy conversion.

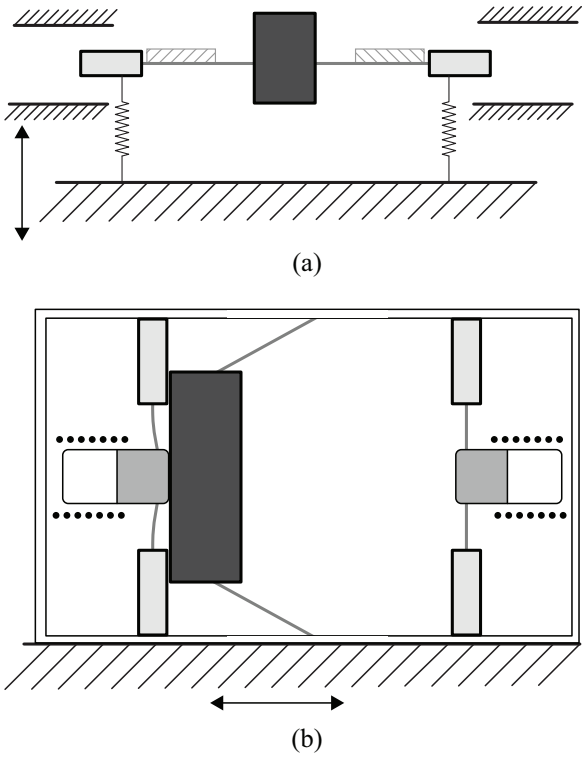

Figure 4. Sketches of frequency up-converting energy harvesters: (a) using impact and (b) using plucking.

3.1.1. Without end-stops. The first group that can be found among the reported devices are the SDoF that operate without end-stops. In Figure 3(a), the working principle of the generator reported by Beeby et al. (2007) is sketched. In this design, a magnet at the tip of a thin beam moves relative to a fixed coil, inducing a current. These generators can be modeled as a linear mass–spring–damper system with mass M, stiffness K, and damping coefficient C. The following equation of motion can be found

$$M\ddot{z} + C\dot{z} + Kz = M\omega^2 Y_0 \sin(\omega t) \tag{4}$$

where z is the relative internal displacement and ω and Y_0 are the frequency and amplitude of the driving motion, respectively. These generators are typically designed to operate at resonance where they greatly amplify the driving motion and achieve high efficiencies.

3.1.2. With soft-stops. Next are the non-linear energy harvesters that rely on a gradually increasing stiffness to limit the internal motion. An example of such a system is the design reported by Geisler et al. (2017), which is sketched in Figure 3(b). In this design, a moving magnet experiences a repulsive force from the oppositely poled magnets at the ends. The dynamics of such a system can be modeled by the Duffing equation shown in equation (5) (Pellegrini et al., 2013)

$$M\ddot{z} + C\dot{z} + \alpha z + \beta z^3 = M\omega^2 Y_0 \sin(\omega t) \tag{5}$$

where α controls the linear stiffness and the stiffening effect is controlled by $\beta>0$. Moreover, systems where $\alpha \geqslant 0$ have one stable position, and a bi-stable system is obtained for $\alpha<0$.

3.1.3. With hard-stops. In the third group, there are the energy harvesters with a very rapid stiffening effect at the end of their range of motion. These stiffening effects are, for example, the result of a mechanical contact, as is the case in the design of Liu et al. (2012), which is sketched in Figure 3(c). In this design, the proof mass mounted on the tip of a piezoelectric beam makes contact with mechanical elements on the top and bottom during excitation. The dynamics of these systems can be modeled by the piecewise linear equation of motion given in equation (6), where C_h and K_h are the damping coefficient and stiffness of the housing, respectively. Solutions to this equation of motion can be found through numerical methods

$$\begin{aligned}
&\text{for } z \geqslant Z_l: \\
&M\ddot{z} + (C + C_h)\dot{z} + (K + K_h)z - K_h Z_l = M\omega^2 Y_0 \sin(\omega t) \\
&\text{for } -Z_l < z < Z_l: \\
&M\ddot{z} + C\dot{z} + Kz = M\omega^2 Y_0 \sin(\omega t) \\
&\text{for } z \leqslant -Z_l: \\
&M\ddot{z} + (C + C_h)\dot{z} + (K + K_h)z + K_h Z_l = M\omega^2 Y_0 \sin(\omega t)
\end{aligned} \tag{6}$$

3.2. Frequency up-converters

In addition, there are systems that use an inertial mass to excite a secondary oscillator in its natural frequency, which is increased w.r.t the frequency of the driving motion. The relative motion of the secondary oscillator is then used for energy conversion.

3.2.1. Using impact. The first group of frequency up-converters (FupC) use the impact of an impact member to excite the secondary oscillators. An example of such a system is the generator reported by Dechant et al. (2017) and is shown in Figure 4(a). In this design, a piezoelectric membrane is mounted between a proof mass (dark) and an impact member (light). Under a driving motion, the impact member is displaced until it makes contact with the mechanical stops at the end of its range of motion. As a result, the proof mass experiences an impulse-like response and begins to oscillate in its own natural frequency. This system can be modeled as a two-DoF system with the following equations of motion

Table 1. The performance properties of the generators categorized in two classes and five groups based on their dynamics.

Class	Group	Motion ratio (λ)	Efficiency (η_{pk})	Bandwidth (BW_{nhe})	References
Single-degree-of-freedom generators	• Without end-stops	27–453	0.08%–27.5%	0.01	Beeby et al. (2007); Huang et al. (2007); Moss et al. (2012)
	• With soft-stops	7.62–409	0.26%–7.72%	0.2–0.58	Geisler et al. (2017); Foisal et al. (2012); Munaz et al. (2013); Salauddin et al. (2016); Saravia et al. (2017); Nammari et al. (2018); Liu et al. (2015b)
	• With hard-stops	0.56–65.9	0.001%–1.17%	0.1–1.78	Liu et al. (2012); Wang et al. (2017); Ashraf et al. (2013a); Ju et al. (2013); Han et al. (2014); Miki et al. (2010)
Frequency up-converters	• Using impact	0.35–14.54	0.011%–0.83%	0.071–0.72	Dechant et al. (2017); Renaud et al. (2009); Halim and Park (2014); Ashraf et al. (2013b)
	• Using plucking	0.025–14.13	0.002%–1.66%	0.336–3.08	Galchev et al. (2011, 2012); Tang et al. (2011); Pillatsch et al. (2012); Halim and Park (2015)

$$\begin{aligned} \text{Eq.6} + C_2 d\dot{z} + K_2 dz &= M\omega^2 Y_0 \sin(\omega t) \\ M_2 \ddot{z}_2 + C_2 d\dot{z} + K_2 dz &= M_2 \omega^2 Y_0 \sin(\omega t) \end{aligned} \tag{7}$$

where Eq.6 is the relevant left side of equation (6), z_2 is the relative internal displacement of the proof mass w.r.t. the housing, $dz = z - z_2$ is the relative internal displacement between the impact member and the proof mass and C_2, K_2, and M_2 are the damping coefficient and stiffness of the connection between the two bodies and the mass of the proof mass, respectively.

3.2.2. Using plucking. The final group contains the FupC that excite their secondary oscillator through plucking. An example was reported by Galchev et al. (2011) and is sketched in Figure 4(b). The design consists of an inertial mass which snaps back and forth between the two secondary oscillators, attaching magnetically. When the inertial mass detaches, the secondary oscillator starts oscillating at its natural frequency and generates power through electromagnetic induction. The dynamics in such a system can be modeled as three oscillators with the following equations of motion

$$\begin{aligned} &\text{Eq.6} + F_u(du) + F_v(dv) = M\omega^2 Y_0 \sin(\omega t) \\ &M_u \ddot{u} + C_u d\dot{u} + K_u u + F_u(du) = M_u \omega^2 Y_0 \sin(\omega t) \\ &M_v \ddot{v} + C_v d\dot{v} + K_v v + F_v(dv) = M_v \omega^2 Y_0 \sin(\omega t) \end{aligned} \tag{8}$$

where u and v and du and dv are the positions of the secondary oscillators w.r.t. the housing and w.r.t. the inertial mass, respectively. M_u, C_u, K_u and M_v, C_v, K_v are the mass, damping coefficient, and stiffness of the secondary oscillators and F_u and F_v are the interaction forces between the secondary oscillator and the inertial mass.

4. Results

Table 1 presents the classification of the reported generators and the calculated values for λ, η_{pk}, and BW_{nhe}. The color coding of the groups is used in Figures 5 and 6, where the motion ratios of the generators are plotted against their peak efficiency η_{pk} and normalized half-efficiency bandwidth BW_{nhe}, respectively. To visualize the domains in which the generators of the different groups were reported, shaded areas were added to the figures. Based on the reported data, the following observations can be made.

4.1. SDoF generators

The majority of the reported generators are of the SDoF class, which covers a widespread in motion ratios, efficiencies, and bandwidths. While efficiencies range from 0.001% to 27.5%, most work reports values between 0.1% and 1%. The normalized half-efficiency bandwidths ranged from 0.01 to 1.78.

4.1.1. Without end-stops. In this group three generators were found. The motion ratios found for this group are at the right of the spectrum presented in Figure 5. It can be observed that within this group the efficiency and motion ratio are correlated. The efficiency of 28% reported by Beeby et al. (2007) is the highest efficiency (according to FoM_G metric) reported in energy harvesting literature. This work was also the only instance where bandwidth information was reported for this group. The half-efficiency bandwidth was 0.53 Hz around a $\omega_{pk} = 52$Hz yielding a normalized half-efficiency bandwidth of $BW_{nhe} = 0.01$.

4.1.2. With soft-stops. The devices with soft-stops were reported seven times with motion ratios ranging

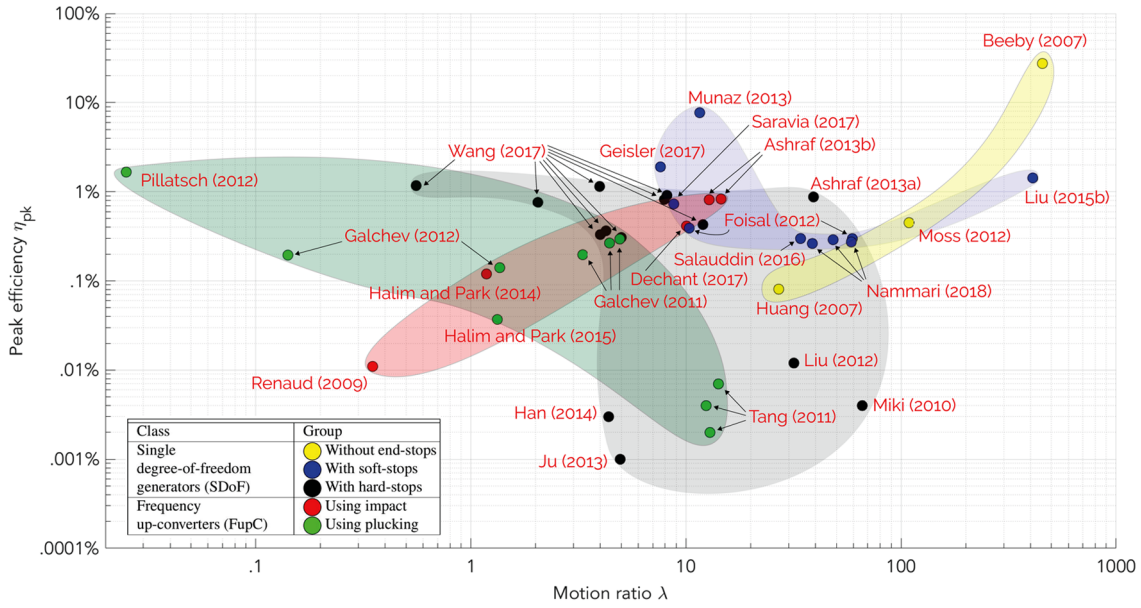

Figure 5. Motion ratio (λ) versus peak efficiency (η_{pk}) of reported generators by generator type. The shaded areas indicate the ranges in which the generators of different groups were reported; multiple arrows originating from one source indicate that a prototype was tested under multiple vibration conditions.

between 7.62 and 409. The efficiencies of these devices ranged from 0.26% to 7.72% and the normalized half-efficiency bandwidths ranged from 0.2 to 0.58. In the work of Salauddin et al. (2016), the effect of the motion ratio on the efficiency was specifically tested by varying the amplitude of the driving motion for a fixed frequency. It was found that when the motion ratio was decreased from 56.81 to 34.09, the efficiency increased from 0.2% to 0.3%.

4.1.3. With hard-stops. In this group six generators were reported. With motion ratios between 0.56 and 65.9 and efficiencies from 0.001% to 1.17%, this group covers a large part of Figure 5. Moreover, in this group normalized half-efficiency bandwidths were reported between 0.1 and 1.78. Wang et al. (2017) reported testing their prototypes under six conditions varying the motion ratios at fixed frequencies and found that for small motion ratios ($\lambda < 1$) a small increase in efficiency was found for their prototypes increased as the motion ratio was increased.

4.2. Frequency up-converters

The FupC class generators are reported predominantly on the left side of Figure 5, with motion ratios of 15 or less. Their motion ratios range from 0.025 to 14.54 and efficiencies are reported between 0.002% and 1.66%. The normalized half-efficiency bandwidths ranged from 0.071 to 3.08.

4.2.1. Using impact. In this group four generators were found. The motion ratios of these devices ranged from 0.35 to 14.54 and their efficiencies between 0.011% and 0.83%. The normalized half-efficiency bandwidths ranged between 0.071 and 0.72. Moreover, the prototype reported by Ashraf et al. (2013b) was also tested for a fixed frequency. When the motion ratio was decreased from 248 to 13, the efficiency increased from 0.088% to 0.83%.

4.2.2. Using plucking. Finally, five examples of frequency up-converters using plucking were found. Their motion ratios ranged from 0.025 to 14.13 and efficiencies between 0.002% and 1.66% were reported. The normalized half-efficiency bandwidths were reported between 0.336 and 3.08. The prototype of Pillatsch et al. (2012) reported the lowest motion ratio and largest normalized bandwidth found in the literature at $\lambda = 0.025$ and $BW_{\text{nhe}} = 3.06$, respectively.

5. Discussion

The widespread in efficiency of the reported energy harvesters can be attributed to the number of variables that contribute to the final efficiency. First of all, there are great differences in the degree of optimization and overall quality of the transduction elements, the mechanical structures, and the power conditioning circuitry. Next, there are great differences in the types of dynamics that are employed and the operating conditions under which they are evaluated.

For example, in linear systems the maximum power output coincides with the maximum efficiency at the resonance point, and it is a common practice to

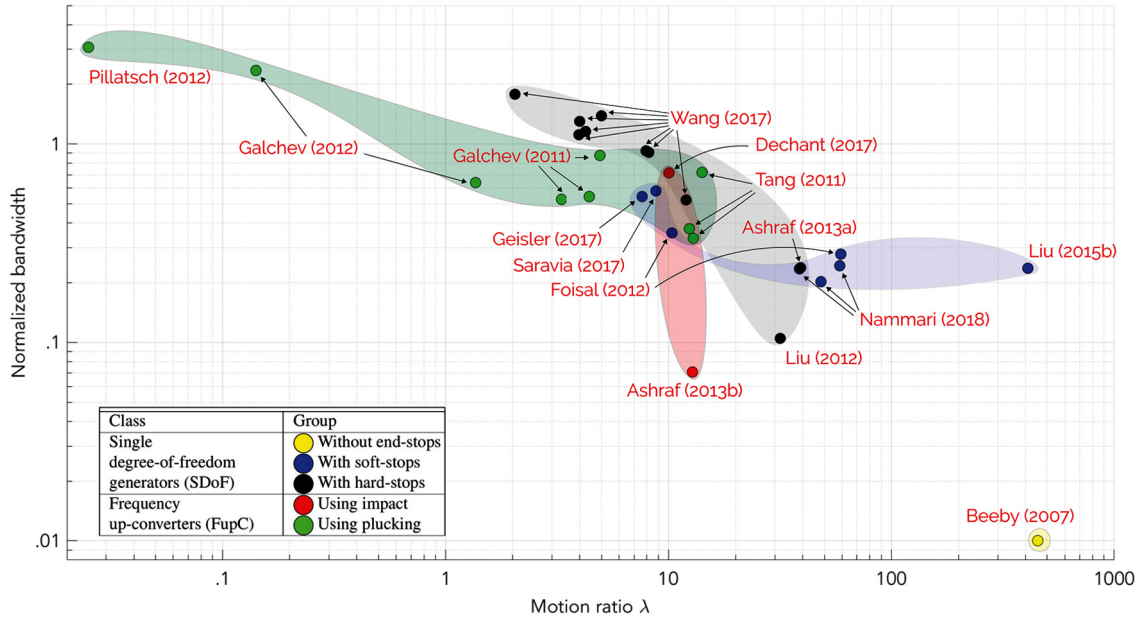

Figure 6. Motion ratio (λ) versus normalized half-efficiency bandwidth (BW_{nhe}) of reported generators by generator type. The shaded areas indicate the ranges in which the generators of different groups were reported; multiple arrows originating from one source indicate that a prototype was tested under multiple vibration conditions.

evaluate the performance at this point. However, for non-linear systems this is not necessarily true and the performance is commonly evaluated at the point of maximum output power, which is not necessarily the point of maximum efficiency. Finally, at least some of the spread can be attributed to the uncertainty that comes with the estimation of some of the parameters that were not explicitly reported by the authors of the experimental work. When the references are grouped by publication year, it can be found that the efficiencies of the reported generators converge over time. This can be an indication of the maturing of the field. Moreover, it is likely that the adoption of established strategies and designs is the main contributor in this aspect.

5.1. SDoF generators

5.1.1. Without end-stops. When generators in this group are driven at resonant condition, amplification of the driving motion is achieved with a ratio that (for $t \to \infty$) only depends on the total damping in the system. Moreover, the portion of output power to the total energy dissipated in the system is only dependent on the ratio between the electrical damping and the parasitic damping. The electrical damping has to be provided by the transduction mechanism and is limited in practice by, for example, magnetic flux density, maximum tensile stress, or dielectric breakdown in electromagnetic, piezoelectric, and electrostatic transducers. As a result, in order to maximize the fraction of useful output power (and thus the efficiency) the amplification factor should be maximized. However, maximizing the amplification factor leads to a very narrow bandwidth, which can also be observed from Figure 6 where the device from this group has by far the smallest normalized bandwidth.

In practice, the upper limit for the amplification factor also depends on the dimensions of the generator and is therefore directly related to the motion ratio of the device. As a result, it can be expected that SDoF generators without end-stops demonstrate higher efficiencies at larger motion ratios. This is supported by the data shown in Figure 5, where a clear correlation is found between efficiency and motion ratio in the SDoF generators without end-stops. Furthermore, none of these systems were found for lower motion ratios, which indicates that these are not favorable conditions for a SDoF system without end-stops.

5.1.2. With soft-stops. Within the group of SDoF generators with soft-stops two embodiments are found. In Figure 5, two groups of points can be observed around $\lambda = 10$ and between $30 < \lambda < 60$. In these devices, the stiffening effect is a result of a magnetic suspension. The footprint of such a suspension is relatively small and therefore these embodiments were found to be relatively efficient in terms of volume. The other embodiment uses a mechanical element to facilitate the stiffening effect. Since the footprint of the mechanical element is relatively large, it was found that the efficiency of this design was lower in terms of volume.

In terms of dynamics, the same principles as with the SDoF generator without end-stops hold. Therefore, it should be expected that higher efficiencies are demonstrated at larger motion ratios. However, the normalized bandwidths of generators using soft-stops are much larger compared to generators without end-stops. In general, the use of soft-stops allows an increased bandwidth and a lower motion ratio and therefore a greater degree of miniaturization at the cost of a reduced efficiency.

5.1.3. With hard-stops. SDoF generators with hard-stops are found in different embodiments and are found in a broad range of motion ratios and efficiencies. Compared to the soft-stop, the ratio between the travel stiffness and the hard-stop stiffness can be extremely large which allows very small motion ratios and therefore a large degree of miniaturization. In general, the kinetic energy of the mass upon engaging the hard-stop is lost which may greatly hurt the efficiency of these systems. In terms of bandwidth, it can be seen from Figure 6 that large normalized bandwidths can be obtained for these devices. Furthermore, it was observed that increased bandwidths are found for lower motion ratios.

5.1.4. Comparison between SDoF generators. Within the class of SDoF generators, it can be observed that the different groups are reported at different ranges of motion ratios, efficiencies, and bandwidths. SDoF generators without end-stops are only reported at larger motion ratios, report the greatest efficiency and the narrowest bandwidth. At very small motion ratios, exclusively SDoF generators with hard-stops were reported. Although their reported bandwidths are much greater, their efficiencies are generally lower due to the loss of kinetic energy when the hard-stops engage. Between those groups the soft-stopped generators are reported. In this group, generators are reported with slightly lower motion ratios compared to those without end-stops, but greater efficiencies compared to those with hard-stops. In general, a correlation can be found between the motion ratio and the efficiency of SDoF generators.

5.2. Frequency up-converters

5.2.1. Using impact. In the group of FupC generators two embodiments can be found. First, there are the systems where an inertial mass impacts on the secondary oscillator. In Figure 5, the two lowest efficiencies of this group are linked to these embodiments. Next, there are the systems where the secondary oscillator is mounted on top of an impact member, which impacts on an end-stop. It was found that these systems reported larger efficiencies compared to the other group.

5.2.2. Using plucking. In the group of plucking FupC generators three embodiments were found. The two generators with the smallest motion ratios made use of a secondary oscillator that was latched magnetically to an inertial body and detached upon excitation. These designs demonstrated the greatest normalized bandwidths of all reported energy harvesters. One design based on mechanical contact was reported and is found in Figure 5 in the middle of the group. The two designs with the largest motion ratios used piezoelectric beams with a magnet at the tip that was repelled by a magnet on the passing inertial mass.

5.2.3. Comparison between FupC generators. Between the groups of FupC no convincing evidence was found that one group would have an advantage compared to the other in terms of motion ratio, efficiency, or bandwidth.

5.3. Comparison between SDoF and FupC generators

The most striking difference between the groups of SDoF and FupC generators is the motion ratio at which they are reported; SDoF systems are mostly reported on the right side of Figure 5, while FupC systems dominate the left side. At the larger motion ratios, the SDoF systems report higher efficiencies compared to the FupC. Reasons for this could be the significantly larger amount of reported work on SDoF generators and the increased complexity of the dynamics of FupC. However, at the lower motion ratios it could be argued that FupC systems may be more efficient than SDoF systems. For example, in the results of the two works of Ashraf et al. (2013a, 2013b), a SDoF generator and FupC are reported with a similar design, shape, and volume and tested under similar conditions. At a motion ratio of approximately $\lambda = 12$, the efficiencies of the SDoF generator and the FupC were 0.30% and 0.80%, respectively.

Another important property of the energy harvester is the bandwidth. Although SDoF generators have the highest peak efficiency, they are very sensitive to changes in the frequency of the driving motion. As a result, their practical use is greatly limited by the narrow range of frequencies where this efficiency is achieved. The non-linearities as a result of the end-stops or the use of a FupC strategy can greatly improve the efficiency over a much wider bandwidth. This can also be clearly observed from the differences between the groups in Figure 6.

5.4. Recommendations

The first recommendation is to consider the motion ratio at an early stage in the design process of the generator, similar to the frequency ratio (ω/ω_n), because

it greatly influences what dynamics can be used in the device. Next, it is recommended for the authors of experimental work on energy harvesters to report at least the following device properties: the dimensions, the total (packaged) volume, the moving mass, and the travel range of the mass. In addition, the following variables should be reported under all test conditions: the frequency and acceleration (or amplitude) of the driving motion and the power output. These parameters are necessary to perform proper analysis of the performance of the reported generator. It may be desirable to evaluate the wideband performance of an energy harvesting system in a single metric. An example of such a metric could be the product of η_{pk} and BW_{nhe}. However, reflecting all these properties in a single figure may lead to the loss of important information and is therefore not recommended as a standalone figure of merit. The last recommendation is to systematically benchmark the performance of typical generator designs under varying conditions and at different scales to gain insight into the design parameters and their sensitivities. This can be used to develop more accurate models to estimate the performance of vibration energy harvesters and will be the focus of future work.

6. Conclusion

Although motion energy harvesting at the small scales has been a research topic for over 20 years, the implementation of such generators remains limited in practice. One of the most important contributing factors here is the poor performance of these devices under low-frequency excitation. In this research, the efficiencies and bandwidths of small-scale generators are studied through two new metrics. The generator figure of merit, FoM_G, is a variation in an existing efficiency metric, which can facilitate a better comparison between generators by making it independent of shape and material. From this metric, the peak efficiency (η_{pk}) and the normalized half-efficiency bandwidth (BW_{nhe}) can be derived and used as important properties to characterize the maximum efficiency and bandwidth of the generator. The motion ratio, λ, is a new metric which describes the relation between the excitation amplitude and the dimension of the generator in the direction of the driving motion. Furthermore, a classification of the dynamics is proposed where the systems are identified as either SDoF generators or FupC and categorized further in one of the five groups. It was found that SDoF generators reported the highest efficiencies, but were mainly found at large motion ratios and had a very narrow bandwidth. Through the use of end-stops lower motion ratios and larger bandwidths could be achieved at the cost of a reduced efficiency. The efficiency of FupC generators was on average found to be lower compared to SDoF systems. However, their typical motion ratios were also much lower and it was found that at these lower motion ratios FupC systems can outperform SDoF generators in terms of both efficiency and bandwidth.

Declaration of conflicting interests

The author(s) declared no potential conflicts of interest with respect to the research, authorship, and/or publication of this article.

Funding

The author(s) disclosed receipt of the following financial support for the research, authorship, and/or publication of this article: This work is part of the research program Rethinking Energy Harvesting for MEMS (REH-MEMS) with project number 14379, which was financed by the Stichting voor de Technische Wetenschappen (STW) and the Netherlands Organization for Scientific Research (NWO).

ORCID iD

Thijs WA Blad https://orcid.org/0000-0002-0280-8121

Note

1. In these figures, the dotted lines indicate the windings of a coil and represent an electromagnetic transducer in combination with the magnets sketched as white-gray rectangles; the gray patches with dashes represent a piezoelectric transducer and the gray lines are flexible elements; the light-gray rectangles are rigid bodies and the dark-gray rectangles are the inertial masses. Finally, the double-sided arrow represents the vibration direction and is imposed in all the points marked as grounded.

References

Ashraf K, Khir MHM, Dennis JO, et al. (2013a) A wideband, frequency up-converting bounded vibration energy harvester for a low-frequency environment. *Smart Materials and Structures* 22(2): 025018. Available at: http://stacks.iop.org/0964-1726/22/i=2/a=025018

Ashraf K, Md Khir MH, Dennis JO, et al. (2013b) Improved energy harvesting from low frequency vibrations by resonance amplification at multiple frequencies. *Sensors and Actuators A: Physical* 195: 123–132. Available at: http://www.sciencedirect.com/science/article/pii/S092442471300143X

Beeby SP, Torah RN, Tudor MJ, et al. (2007) A micro electromagnetic generator for vibration energy harvesting. *Journal of Micromechanics and Microengineering* 17(7): 1257. Available at: http://stacks.iop.org/0960-1317/17/i=7/a=007

Bowers BJ and Arnold DP (2009) Spherical, rolling magnet generators for passive energy harvesting from human motion. *Journal of Micromechanics and Microengineering* 19(9): 094008. Available at: http://stacks.iop.org/0960-1317/19/i=9/a=094008

Daqaq MF, Masana R, Erturk A, et al. (2014) On the role of nonlinearities in vibratory energy harvesting: a critical

review and discussion. *Applied Mechanics Reviews* 66(4): 040801.

Dechant E, Fedulov F, Chashin DV, et al. (2017) Low-frequency, broadband vibration energy harvester using coupled oscillators and frequency up-conversion by mechanical stoppers. *Smart Materials and Structures* 26(6): 065021. Available at: http://stacks.iop.org/0964-1726/26/i=6/a=065021

Foisal ARM, Hong C and Chung GS (2012) Multi-frequency electromagnetic energy harvester using a magnetic spring cantilever. *Sensors and Actuators A: Physical* 182: 106–113. Available at: http://www.sciencedirect.com/science/article/pii/S0924424712002865

Galchev T, Aktakka EE and Najafi K (2012) A piezoelectric parametric frequency increased generator for harvesting low-frequency vibrations. *Journal of Microelectromechanical Systems* 21(6): 1311–1320.

Galchev T, Kim H and Najafi K (2011) Micro power generator for harvesting low-frequency and nonperiodic vibrations. *Journal of Microelectromechanical Systems* 20(4): 852–866.

Geisler M, Boisseau S, Perez M, et al. (2017) Human-motion energy harvester for autonomous body area sensors. *Smart Materials and Structures* 26(3): 035028. Available at: http://stacks.iop.org/0964-1726/26/i=3/a=035028

Green PL, Papatheou E and Sims ND (2013) Energy harvesting from human motion and bridge vibrations: an evaluation of current nonlinear energy harvesting solutions. *Journal of Intelligent Material Systems and Structures* 24(12): 1494–1505.

Halim MA and Park JY (2014) Theoretical modeling and analysis of mechanical impact driven and frequency up-converted piezoelectric energy harvester for low-frequency and wide-bandwidth operation. *Sensors and Actuators A: Physical* 208: 56–65. Available at: http://linkinghub.elsevier.com/retrieve/pii/S0924424713006316

Halim MA and Park JY (2015) Modeling and experiment of a handy motion driven, frequency up-converting electromagnetic energy harvester using transverse impact by spherical ball. *Sensors and Actuators A: Physical* 229: 50–58. Available at: http://www.sciencedirect.com/science/article/pii/S0924424715001478

Han M, Yuan Q, Sun X, et al. (2014) Design and fabrication of integrated magnetic MEMS energy harvester for low frequency applications. *Journal of Microelectromechanical Systems* 23(1): 204–212.

Huang WS, Tzeng KE, Cheng MC, et al. (2007) A silicon mems micro power generator for wearable micro devices. *Journal of the Chinese Institute of Engineers* 30(1): 133–140.

Ju S, Chae SH, Choi Y, et al. (2013) A low frequency vibration energy harvester using magnetoelectric laminate composite. *Smart Materials and Structures* 22(11): 115037. Available at: http://stacks.iop.org/0964-1726/22/i=11/a=115037

Kulah H and Najafi K (2008) Energy scavenging from low-frequency vibrations by using frequency up-conversion for wireless sensor applications. *IEEE Sensors Journal* 8(3): 261–268.

Liu H, Lee C, Kobayashi T, et al. (2012) A new S-shaped MEMS PZT cantilever for energy harvesting from low frequency vibrations below 30 Hz. *Microsystem Technologies* 18(4): 497–506. Available at: https://link.springer.com/article/10.1007/s00542-012-1424-1

Liu W, Badel A, Formosa F, et al. (2015a) A new figure of merit for wideband vibration energy harvesters. *Smart Materials and Structures* 24(12): 125012.

Liu W, Badel A, Formosa F, et al. (2015b) A wideband integrated piezoelectric bistable generator: experimental performance evaluation and potential for real environmental vibrations. *Journal of Intelligent Material Systems and Structures* 26(7): 872–877.

Miki D, Honzumi M, Suzuki Y, et al. (2010) Large-amplitude MEMS electret generator with nonlinear spring. In: *2010 IEEE 23rd international conference on micro electro mechanical systems (MEMS)*, 24–28 January, Wan Chai, Hong Kong, pp. 176–179. New York: IEEE.

Mitcheson PD, Yeatman EM, Rao GK, et al. (2008) Energy harvesting from human and machine motion for wireless electronic devices. *Proceedings of the IEEE* 96(9): 1457–1486.

Moss SD, McLeod JE, Powlesland IG, et al. (2012) A bi-axial magnetoelectric vibration energy harvester. *Sensors and Actuators A: Physical* 175: 165–168. Available at: http://www.sciencedirect.com/science/article/pii/S0924424711007370

Munaz A, Lee BC and Chung GS (2013) A study of an electromagnetic energy harvester using multi-pole magnet. *Sensors and Actuators A: Physical* 201: 134–140. Available at: http://www.sciencedirect.com/science/article/pii/S0924424713003191

Nammari A, Caskey L, Negrete J, et al. (2018) Fabrication and characterization of non-resonant magneto-mechanical low-frequency vibration energy harvester. *Mechanical Systems and Signal Processing* 102: 298–311. Available at: http://www.sciencedirect.com/science/article/pii/S0888327017305198

Pellegrini SP, Tolou N, Schenk M, et al. (2013) Bistable vibration energy harvesters: a review. *Journal of Intelligent Material Systems and Structures* 24(11): 1303–1312.

Pillatsch P, Yeatman EM and Holmes AS (2012) A scalable piezoelectric impulse-excited energy harvester for human body excitation. *Smart Materials and Structures* 21(11): 115018. Available at: http://stacks.iop.org/0964-1726/21/i=11/a=115018

Renaud M, Fiorini P, Schaijk Rv, et al. (2009) Harvesting energy from the motion of human limbs: the design and analysis of an impact-based piezoelectric generator. *Smart Materials and Structures* 18(3): 035001. Available at: http://stacks.iop.org/0964-1726/18/i=3/a=035001

Roundy S (2005) On the effectiveness of vibration-based energy harvesting. *Journal of Intelligent Material Systems and Structures* 16(10): 809–823.

Salauddin M, Halim MA and Park JY (2016) A magnetic spring-based, low-frequency-vibration energy harvester comprising a dual Halbach array. *Smart Materials and Structures* 25(9): 095017. Available at: http://stacks.iop.org/0964-1726/25/i=9/a=095017

Saravia CM, Ramrez JM and Gatti CD (2017) A hybrid numerical-analytical approach for modeling levitation based vibration energy harvesters. *Sensors and Actuators A: Physical* 257: 20–29. Available at: http://www.sciencedirect.com/science/article/pii/S0924424716306483

Tang QC, Yang YL and Li X (2011) Bi-stable frequency up-conversion piezoelectric energy harvester driven by non-contact magnetic repulsion. *Smart Materials and Structures* 20(12): 125011. Available at: http://stacks.iop.org/0964-1726/20/i=12/a=125011

Wang Y, Zhang Q, Zhao L, et al. (2017) Non-resonant electromagnetic broad-band vibration-energy harvester based on self-assembled ferrofluid liquid bearing. *Journal of Microelectromechanical Systems* 26(4): 809–819.

Williams CB and Yates RB (1996) Analysis of a micro-electric generator for microsystems. *Sensors and Actuators A: Physical* 52(1): 8–11. Available at: http://www.sciencedirect.com/science/article/pii/092442479680118X